All-optical non-volatile tuning of AMZI-coupled ring resonator with GST phase-change material

HANYU ZHANG[1], LINJIE ZHOU[1*], JIAN XU[1], LIANGJUN LU[1], JIANPING CHEN[1], AND B. M. A. RAHMAN[2]

[1]State Key Laboratory of Advanced Optical Communication Systems and Networks, Shanghai Institute for Advanced Communication and Data Science, Department of Electronic Engineering, Shanghai Jiao Tong University, Shanghai 200240, China
[2]Department of Electrical and Electronic Engineering, City, University of London, London EC 1V 0HB, U.K.
*Corresponding author: ljzhou@sjtu.edu.cn

Received XX Month XXXX; revised XX Month, XXXX; accepted XX Month XXXX; posted XX Month XXXX (Doc. ID XXXXX); published XX Month XXXX

We present a $Ge_2Sb_2Te_5$(GST)-integrated ring resonator with the tuning enabled by all-optical phase change of GST using a sequence of optical pulses. The tuning is non-volatile and repeatable, with no static power consumption due to the "self-holding" feature of the GST phase-change material. The 2-μm-long GST can be partially crystallized by controlling the number of pulses, increasing the tuning freedom. The coupling between the ring resonator and the bus waveguide is based on an asymmetric Mach-Zehnder interferometer. The coupling strength is wavelength-dependent so that an optimal wavelength can be selected for the probe light to get more than 20 dB transmission contrast between the amorphous and crystalline GST states. © 2018 Optical Society of America

OCIS codes: *(230.4555) Coupled resonators; (160.2900) Optical storage materials; (160.3130) Integrated optics materials; (230.3120) Integrated optics devices.*

http://dx.doi.org/10.1364/OL.99.099999

The active tuning of silicon photonic devices is mostly achieved by the thermo-optic (TO) effect or the electro-optic (EO) effect based on free-carrier injection, which has a refractive index (RI) tuning range in the order of 0.01 and 0.001, respectively. Thus, in order to obtain adequate phase change, usually, a relative long waveguide of 100's μm to mm length is required [1], although there are some exceptional cases such as very efficient TO phase shifter [2] and silicon-plasmonic-organic hybrid phase shifters [3]. Additional energy is also needed to maintain the elevated temperature in the TO tuning or the current injection in the EO tuning. Phase-change materials (PCMs) offer an extremely large RI tuning range with non-volatile phase states. In recent years, the ability to switch rapidly and reversibly between amorphous and crystalline states of a PCM with significantly different optical and electronic properties has found an increasingly wider variety of potential applications in photonics such as neuromorphic computing, multi-level storage, display, and photonic in-memory computing [4-8]. The prototypical phase-change material $Ge_2Sb_2Te_5$ (GST) exhibits distinct optical and electrical properties in its amorphous, metastable distorted face-centered cubic (FCC), and hexagonal forms. High speed and reversible phase transitions between two states could be triggered by thermal [9], optical [10, 11] or electrical pulses [12, 13]. In addition, this material possesses the "self-holding" feature so it does not require static power to maintain the states [14]. This feature can be utilized to implement reconfigurable, non-volatile and low-power optical devices.

In this letter, we investigate a silicon asymmetric Mach-Zehnder interferometer (AMZI)-coupled ring resonator integrated with GST material for all-optical resonance tuning. The AMZI coupler makes it possible to achieve critical coupling at certain wavelengths, offering a large switching extinction ratio upon GST phase change. It points to a new way of creating energy-efficient non-volatile optical components towards large-scale silicon photonic hybrid integration.

Figure 1(a) illustrates the structure of the GST-loaded silicon waveguide. The single-mode silicon waveguide height is h = 220 nm and width is w = 500 nm with air upper-cladding and 2-μm-thick buried oxide under-cladding. A stack of 15-nm-thick GST layer and 10-nm-thick indium tin oxide (ITO) layer with a length of L_{GST} is placed on top of the silicon waveguide to form a hybrid waveguide. The ITO layer is used to protect the GST from being oxidized when it is exposed in the atmosphere environment [15]. The GST phase change is reversible and repeatable, as shown in Fig. 1(b). In the crystallization process, only even-numbered rings are constructed from amorphous GST (a-GST). In the re-amorphization process, the a-GST can be converted to the crystal GST (c-GST), which only transforms the large-size even-numbered (8-, 10-, 12-fold) rings to NaCl-type structure (4-and 6-fold rings). In this process, the Ge/Sb–Te bonds are formed but no bond is broken, leading to the fast crystallization of the amorphous phase [16]. The significant change in bonds results in a great difference in RI between the amorphous and crystalline states. The high contrast in the optical property means that the optical transmission through the GST-loaded

waveguide can be efficiently modulated by changing the GST phase state. Figure 1(c) illustrates the modal electric-field intensity profiles for the GST-loaded silicon waveguide in two phase states. The refractive indices of silicon and silica are taken as 3.481 and 1.445, respectively. The complex refractive index of ITO is 1.55+0.33i. The complex refractive index of GST is taken as 3.9207+0.0055i and 6.0769+0.9040i for the amorphous and crystalline states, respectively [17]. In the amorphous phase, the optical field is mainly confined in the silicon waveguide, with an effective index of 2.516+0.0067i for the transverse electric (TE) polarization. In the crystalline state, on the other hand, the optical field is localized more in the GST layer, with a larger effective index of 2.693 + 0.111i. Thus, the crystalline state has a larger propagation constant and a higher optical absorption loss.

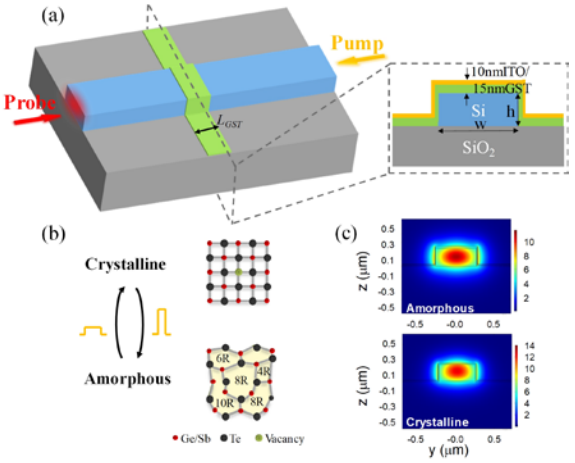

Fig. 1. (a) Schematic structure of the GST-loaded silicon waveguide. The inset shows the cross-sectional view of the Si-GST hybrid waveguide section. (b) Reversible phase change of GST material. (c) Simulated modal electric-field profiles of the Si-GST hybrid waveguide for the two phase states.

The GST-loaded silicon waveguide can be integrated into a ring resonator to control its resonance property. Figure 2(a) shows the structure of a ring resonator with coupling enabled by an AMZI coupler. The ring resonator feedback waveguide is covered with a small patch of GST. The AMZI is composed of two 3-dB 2×2 multimode interferometers (MMIs) connected by a pair of waveguides of different lengths.

The key advantage of our AMZI-coupled ring resonator lies in its strong wavelength dependence of coupling on wavelength, so different coupling conditions are obtained in a small wavelength range. We make full use of this merit in our pump-probe all-optical resonance tuning experiment. The pump pulse is chosen to be in the over-coupling regime so that it can interact with the GST without suffering the narrow band filtering effect of the ring resonator. On the other hand, the probe light is chosen at the critical-coupling wavelength which gives the maximum optical transmission contrast between the amorphous and crystalline states.

The transfer matrix of the MZI coupler is given by

$$M = \begin{pmatrix} t & \kappa \\ \kappa & -t \end{pmatrix} \quad (1)$$

$$t = \frac{1}{2}A_1 \cdot \exp(j\varphi_1)) - \frac{1}{2}A_2 \cdot \exp(j\varphi_2) \quad (2)$$

$$\kappa = -\frac{1}{2}j \cdot A_1 \cdot \exp(j\varphi_1) + \frac{1}{2}j \cdot A_2 \cdot \exp(j\varphi_2) \quad (3)$$

where A_1 (A_2) and φ_1 (φ_2) represent the amplitude and phase of the optical field transmission through the long (short) arm, respectively.

The input-normalized output electric-field transfer function can be expressed as:

$$\left|\frac{b_1}{a_1}\right|^2 = \left|t + \frac{\kappa^2 A_3 \exp(j\varphi_3)}{1 - A_3 t \exp(j\varphi_3)}\right|^2 \quad (4)$$

where a_i and b_i (i = 1, 2) are the electric fields before and after the AMZI coupler, respectively, A_3 and φ_3 represent the amplitude and phase of the optical field transmission through the ring feedback waveguide, respectively. The phase change of GST will modify both the optical phase, φ_3 (RI real part change) and the optical transmission amplitude, A_3 (RI imaginary part change) in (4).

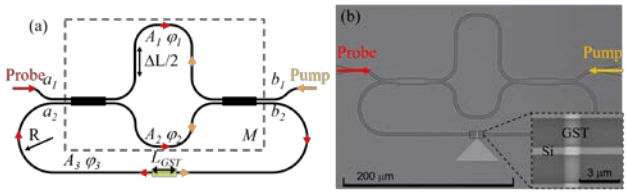

Fig. 2. (a) Schematic structure of the AMZI-coupled ring resonator integrated with GST. (b) Scanning electron microscope image of the fabricated device. The inset shows the zoom-in of the GST-loaded ring waveguide.

The device was fabricated in a silicon-on-insulator (SOI) wafer with the top silicon layer thickness of 220 nm. The silicon waveguide patterns were defined using e-beam lithography (EBL) and subsequent reactive ion etch (RIE). The etch depth was 220 nm, down to the buried oxide under-cladding layer. A second EBL was used to open the GST deposition window. GST was sputtered from a stoichiometric GST target, immediately followed by ITO sputtering deposition to protect the GST. Finally, the device was placed in an acetone bath for lift-off stripping so that the GST/ITO was only left in the deposition window. Figure 2(b) shows the scanning electron microscope (SEM) image of the AMZI-coupled ring resonator covered with a small piece of GST. The length of GST is L_{GST} = 2 μm. The length difference between the AMZI two arms is ΔL = 70 μm. The waveguide cross-sectional dimensions are the same as those used in the Fig. 1.

We used a pump-probe experimental setup as sketched in Fig. 3 (a) to measure the ring resonator transmission spectrum upon GST phase change. The pump pulses were obtained by modulating the continuous-wave (CW) laser light using an electro-optical modulator (EOM) driven by an arbitrary waveform generator (AWG). The pump pulses were subsequently amplified to reach the appropriate peak power. The probe light was from another CW laser with the optical power fixed to a lower level (-6 dBm) so that the device spectrum could be measured without changing the GST phase state. The pump light and the probe light were separated by two optical circulators. The probe light after the device was switched for static and dynamic measurements. In the static

transmission spectrum measurement, the probe light was directly detected by an optical detector. For the dynamic response measurement, the probe light was further amplified and then detected by a high-speed photodiode before being received by an oscilloscope. The pump light and probe light were set to the TE polarization using polarization controllers (PC) prior to coupling to the device. Figure 3(b) shows the typical waveform of the pump pulses. The pulse was measured before coupling to the chip. The coupling loss of the grating coupler is around 5 dB/facet.

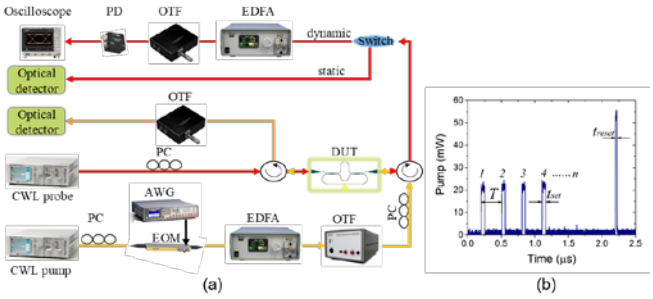

Fig. 3. (a) Optical pump & probe experimental setup for characterizing the device. CWL: continuous-wave laser; PC: polarization controller; AWG: arbitrary waveform generator; EOM: electro-optic modulator; EDFA: erbium-doped fiber amplifier; OTF: optical tunable filter; DUT: device under test; PD: photodiode. (b) Typical pump signal waveform showing both set and reset pulses.

We first measured the transmission spectrum of the device with the probe laser wavelength scanning from 1520 to 1580 nm. Figure 4(a) shows the transmission spectra for two phase-change cycles (two crystalline states and two amorphous states). The spectra were normalized to a reference straight waveguide. The crystallization of GST was induced by a sequence of identical optical pulses with a width t_{set} = 50 ns and peak power P_{set} = 21 mW. The pump light is set to 1556.6 nm (κ close to 1). Each of these pulses initiated partial crystallization of the GST. Subsequently, the re-amorphization was induced by a single pulse with a width t_{reset} = 20 ns and peak power P_{reset} = 53 mW at the same wavelength. The two amorphous state spectra and the two crystalline state spectra are both well overlapped, indicating good repeatability of the resonance tuning using GST phase change. Figure 4(b) illustrates the four intermediate states ($state_1$ to $state_4$) of the crystallization process. It can be seen that the resonance spectrum gradually evolves when the GST goes through the intermediate states.

In order to illustrate the resonant enhancement effect on the transmission contrast upon GST phase change, we also measured a GST-loaded straight waveguide as a comparison. The dimensions of the silicon waveguide and the GST are the same as the AMZI device. Figure 4(c) shows the normalized transmission spectra of the straight waveguide over two phase change cycles.

We define the transmission contrast as the output power difference between the amorphous and crystalline states. Figure 4(d) shows the transmission contrast of the ring resonator and the straight waveguide as a function of wavelength. The maximum contrast of the ring resonator is larger than 20 dB, achieved at the critical coupling wavelengths of either amorphous or crystalline state. In contrast, the transmission contrast of the waveguide is only 5 dB, although it is wavelength independent.

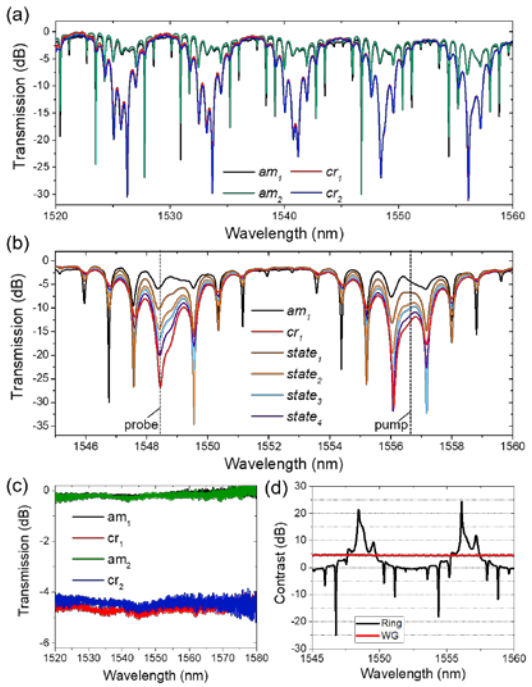

Fig. 4. (a) Measured transmission spectra of the ring resonator device over two phase-change cycles. (b) Intermediate transmission spectra when the GST is partially crystallized. (c) Measured transmission spectra of a GST-loaded straight waveguide over two phase-change cycles. (d) Transmission contrast between the crystalline and amorphous states.

We next investigated the time response of the output transmission upon phase change. The probe light was fixed at 1548.4 nm to get the maximum transmission contrast. The initial phase of GST was amorphous and the partial crystallization of GST by controlling the width of pump pulses t_{set} and the number of pump pulses n generated multiple intermediate levels. The period of the crystallization pulse T is fixed at 300 ns. Figures 5 (a)-(c) show that four, six and seven clearly distinguishable intermediate levels can be obtained, respectively, due to the partial crystallization of GST. The width of the pump pulses is t_{set} = 50ns and 40ns for the four and six levels, respectively. When a re-amorphization pulse was applied, the transmission rises to the initial level as GST became amorphous. Therefore, as long as the energy of the reset pulse is sufficiently large, the GST in an arbitrary intermediate state can return to the original amorphous state. In Fig. 5 (c), the width of pump pulses t_{set} = 40 ns and the number of pump pulses n=10. As GST was completely crystallized after the first eight pulses, only seven intermediate states were eventually obtained. Figure 5 (d) shows the measured time response when only a single crystallization pulse was applied. The probe light power first drops rapidly and then rises slightly until it is completely stable. The gradual increase of the transmission after phase change is due to the heating effect [8].

The parameters of the ring resonator can be extracted by fitting the measured spectra using (4). Table 1 summarizes the extracted parameters for various GST states. The extinction coefficients of the GST-loaded silicon waveguide are k_{eff} = 0.03881 and 0.2161 for the amorphous and crystalline states, respectively. The measurement gives larger losses than simulation, which may be caused by several factors. First, the surface roughness of GST and ITO films could

cause additional scattering loss. Second, in the simulation, we did not consider the refractive index change of the ITO material affected by the pump pulses. In fact, the conductance and loss of ITO increase after high-temperature annealing by the pump pulses [18]. From the amorphous to the crystalline state, the effective index increases by n_{eff} = 0.07436. This presents a larger RI tuning range compared to the thermo-optic or electro-optic effects in silicon. The measured effective index change is slightly smaller than the simulation. It could be caused by the insufficient crystallization or re-amorphization of GST by a sequence of equal-energy pump pulses. Crystallization pulses need to be further optimized to have continuously decreased energy, which is worth further investigation in the future work.

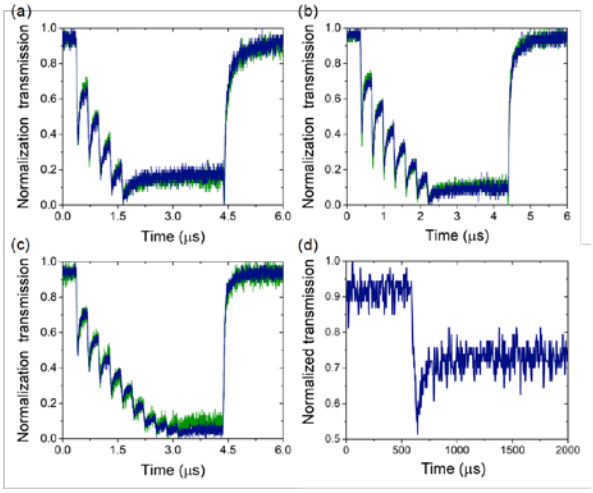

Fig. 5. (a-c) Temporal response of the device when a sequence of crystallization pulses followed by a single re-amorphization pulse is applied. Multiple clearly distinguishable intermediate levels of (a) four, (b) six and (c) seven stairs can be discerned. Two measurements were performed to illustrate its repeatability. (d) Temporal response when a single crystallization pulse is applied.

TABLE I. Extracted Microring Resonator Parameters When GST Is at the Various States.

state	A_3	k_{eff}	$\Delta\varphi_3$	Δn_{eff}
am_1	0.7311	0.03881	Reference	
$state_1$	0.4801	0.09091	0.1164	0.01439
$state_2$	0.3455	0.1317	0.2327	0.02878
$state_3$	0.2941	0.1516	0.3103	0.03838
$state_4$	0.2360	0.1789	0.4266	0.05277
cr_1	0.1748	0.2161	0.6012	0.07436

In conclusion, we have investigated a silicon AMZI-coupled ring resonator integrated with a small piece of GST material on top of the ring waveguide. The phase-change of GST provides a new tool to tune the resonance with the "self-holding" feature. The partial crystallization of GST by controlling the number of pump pulses also allows for the presence of multiple intermediate states. This gives an effective tool to manipulate light propagation with the phase-change material in integrated photonic devices. The comparison of our device with the straight waveguide clearly indicates that the ring resonator has a much more sensitive transmission response to GST phase change than that of the straight waveguide at the critical coupling wavelengths. The ring resonance greatly improves the switching extinction ratio. No energy is required to maintain the GST phase state. These results open the way for a new class of all-optically non-volatile silicon photonic devices. The GST material that we used is just one type of candidate phase-change material. In fact, there exist a great variety of other phase-change materials, such as vanadium dioxide [19], $Ge_2Sb_2Se_4Te_1$ [20], etc. They could be further explored in the future work to realize high-speed and low-loss all-optical devices.

ACKNOWLEDGMENT. This work was supported in part by the National Natural Science Foundation of China (NSFC) (61535006, 61705129, 61661130155).

References

1. L. Lu, S. Zhao, L. Zhou, D. Li, Z. Li, M. Wang, X. Li, and J. Chen, Opt. Express **24**, 9295-9307 (2016).
2. M. R. Watts, J. Sun, C. DeRose, D. C. Trotter, R. W. Young, and G. N. Nielson, Opt. Lett. **38**, 733-735 (2013).
3. W. Heni, C. Haffner, B. Baeuerle, Y. Fedoryshyn, A. Josten, D. Hillerkuss, J. Niegemann, A. Melikyan, M. Kohl, D. L. Elder, L. R. Dalton, C. Hafner, and J. Leuthold, J. Lightwave Technol. **34**, 393-400 (2016).
4. Z. Cheng, C. Rios, N. Youngblood, C. D. Wright, W. H. P. Pernice, and H. Bhaskaran, Adv. Mater. **30**, e1802435 (2018).
5. J. Feldmann, M. Stegmaier, N. Gruhler, C. Rios, H. Bhaskaran, C. D. Wright, and W. H. P. Pernice, Nat. Commun. **8**, 1256 (2017).
6. P. Hosseini, C. D. Wright, and H. Bhaskaran, Nature **511**, 206-211 (2014).
7. D. Kuzum, R. G. Jeyasingh, B. Lee, and H. S. Wong, Nano Lett. **12**, 2179-2186 (2012).
8. C. Ríos, M. Stegmaier, P. Hosseini, D. Wang, T. Scherer, C. D. Wright, H. Bhaskaran, and W. H. P. Pernice, Nat. Photonics **9**, 725-732 (2015).
9. M. Stegmaier, C. Ríos, H. Bhaskaran, and W. H. P. Pernice, ACS Photonics **3**, 828-835 (2016).
10. M. Rudé, J. Pello, R. E. Simpson, J. Osmond, G. Roelkens, J. J. G. M. van der Tol, and V. Pruneri, Appl. Phys. Lett. **103**, 141119 (2013).
11. J. Zheng, A. Khanolkar, P. Xu, S. Colburn, S. Deshmukh, J. Myers, J. Frantz, E. Pop, J. Hendrickson, J. Doylend, N. Boechler, and A. Majumdar, Opt. Mater. Express **8**, 1551 (2018).
12. K. Kato, M. Kuwahara, H. Kawashima, T. Tsuruoka, and H. Tsuda, Appl. Phys. Express **10**, 072201 (2017).
13. A. Aboujaoude, J. Burrow, J. Hendrickson, I. Agha, A. Sarangan, and J. W. Haus, in *Conference on Lasers and Electro-Optics 2018* (Optical Society of America, 2018), paper JW2A.105.
14. K.-K. Du, Q. Li, Y.-B. Lyu, J.-C. Ding, Y. Lu, Z.-Y. Cheng, and M. Qiu, Light-Sci. Appl. **6**, e16194-e16194 (2016).
15. A. Redaelli, *Phase Change Memory Device Physics Reliability and Applications* (Springer, 2018).
16. S. Kohara, K. Kato, S. Kimura, H. Tanaka, T. Usuki, K. Suzuya, H. Tanaka, Y. Moritomo, T. Matsunaga, N. Yamada, Y. Tanaka, H. Suematsu, and M. Takata, Appl. Phys. Lett. **89**, 201910 (2006).
17. H. Zhang, L. Zhou, B. M. A. Rahman, X. Wu, L. Lu, Y. Xu, J. Xu, J. Song, Z. Hu, L. Xu, and J. Chen, IEEE Photonics J. **10**, 1-10 (2018).
18. Y. Hu, X. Diao, C. Wang, W. Hao, and T. Wang, Vacuum **75**, 183-188 (2004).
19. K. J. Miller, K. A. Hallman, R. F. Haglund, and S. M. Weiss, Opt. Express **25**, 26527-26536 (2017).
20. Q. Zhang, Y. Zhang, J. Li, R. Soref, T. Gu, and J. Hu, Opt. Lett. **43**, 94-97 (2018).

1. L. Lu, S. Zhao, L. Zhou, D. Li, Z. Li, M. Wang, X. Li, and J. Chen, "16 x 16 non-blocking silicon optical switch based on electro-optic Mach-Zehnder interferometers," Opt. Express **24**, 9295-9307 (2016).
2. M. R. Watts, J. Sun, C. DeRose, D. C. Trotter, R. W. Young, and G. N. Nielson, "Adiabatic thermo-optic Mach-Zehnder switch," Opt. Lett. **38**, 733-735 (2013).
3. W. Heni, C. Haffner, B. Baeuerle, Y. Fedoryshyn, A. Josten, D. Hillerkuss, J. Niegemann, A. Melikyan, M. Kohl, D. L. Elder, L. R. Dalton, C. Hafner, and J. Leuthold, "108 Gbit/s plasmonic Mach–Zehnder modulator with > 70-GHz electrical bandwidth," J. Lightwave Technol. **34**, 393-400 (2016).
4. Z. Cheng, C. Rios, N. Youngblood, C. D. Wright, W. H. P. Pernice, and H. Bhaskaran, "Device-Level photonic memories and logic applications using phase-change materials," Adv. Mater. **30**, e1802435 (2018).
5. J. Feldmann, M. Stegmaier, N. Gruhler, C. Rios, H. Bhaskaran, C. D. Wright, and W. H. P. Pernice, "Calculating with light using a chip-scale all-optical abacus," Nat. Commun. **8**, 1256 (2017).
6. P. Hosseini, C. D. Wright, and H. Bhaskaran, "An optoelectronic framework enabled by low-dimensional phase-change films," Nature **511**, 206-211 (2014).
7. D. Kuzum, R. G. Jeyasingh, B. Lee, and H. S. Wong, "Nanoelectronic programmable synapses based on phase change materials for brain-inspired computing," Nano Lett. **12**, 2179-2186 (2012).
8. C. Ríos, M. Stegmaier, P. Hosseini, D. Wang, T. Scherer, C. D. Wright, H. Bhaskaran, and W. H. P. Pernice, "Integrated all-photonic non-volatile multi-level memory," Nat. Photonics **9**, 725-732 (2015).
9. M. Stegmaier, C. Ríos, H. Bhaskaran, and W. H. P. Pernice, "Thermo-optical effect in phase-change nanophotonics," ACS Photonics **3**, 828-835 (2016).
10. M. Rudé, J. Pello, R. E. Simpson, J. Osmond, G. Roelkens, J. J. G. M. van der Tol, and V. Pruneri, "Optical switching at 1.55 μm in silicon racetrack resonators using phase change materials," Appl. Phys. Lett. **103**, 141119 (2013).
11. J. Zheng, A. Khanolkar, P. Xu, S. Colburn, S. Deshmukh, J. Myers, J. Frantz, E. Pop, J. Hendrickson, J. Doylend, N. Boechler, and A. Majumdar, "GST-on-silicon hybrid nanophotonic integrated circuits: a non-volatile quasi-continuously reprogrammable platform," Opt. Mater. Express **8**, 1551 (2018).
12. K. Kato, M. Kuwahara, H. Kawashima, T. Tsuruoka, and H. Tsuda, "Current-driven phase-change optical gate switch using indium–tin-oxide heater," Appl. Phys. Express **10**, 072201 (2017).
13. A. Aboujaoude, J. Burrow, J. Hendrickson, I. Agha, A. Sarangan, and J. W. Haus, "Influence of geometry on speed of phase-change in GST-based nanorods," *in Conference on Lasers and Electro-Optics 2018* (Optical Society of America, 2018), paper JW2A.105.
14. K.-K. Du, Q. Li, Y.-B. Lyu, J.-C. Ding, Y. Lu, Z.-Y. Cheng, and M. Qiu, "Control over emissivity of zero-static-power thermal emitters based on phase-changing material GST," Light-Sci. Appl. **6**, e16194-e16194 (2016).
15. A. Redaelli, *Phase Change Memory Device Physics, Reliability and Applications* (Springer, 2018).
16. S. Kohara, K. Kato, S. Kimura, H. Tanaka, T. Usuki, K. Suzuya, H. Tanaka, Y. Moritomo, T. Matsunaga, N. Yamada, Y. Tanaka, H. Suematsu, and M. Takata, "Structural basis for the fast phase change of $Ge_2Sb_2Te_5$: Ring statistics analogy between the crystal and amorphous states," Appl. Phys. Lett. **89**, 201910 (2006).
17. H. Zhang, L. Zhou, B. M. A. Rahman, X. Wu, L. Lu, Y. Xu, J. Xu, J. Song, Z. Hu, L. Xu, and J. Chen, "Ultracompact Si-GST hybrid waveguides for nonvolatile light wave manipulation," IEEE Photonics J. **10**, 1-10 (2018).
18. Y. Hu, X. Diao, C. Wang, W. Hao, and T. Wang, "Effects of heat treatment on properties of ITO films prepared by rf magnetron sputtering," Vacuum **75**, 183-188 (2004).
19. K. J. Miller, K. A. Hallman, R. F. Haglund, and S. M. Weiss, "Silicon waveguide optical switch with embedded phase change material," Opt. Express **25**, 26527-26536 (2017).
20. Q. Zhang, Y. Zhang, J. Li, R. Soref, T. Gu, and J. Hu, "Broadband nonvolatile photonic switching based on optical phase change materials: beyond the classical figure-of-merit," Opt. Lett. **43**, 94-97 (2018).